Darrieus wind turbine noise propagation in urban environments using ray tracing

Kartik Venkatraman, Andrea C Bresciani, Julien Maillard, Stéphane Moreau, Julien Christophe, Christophe F Schram

AIAA AVIATION Forum
12-16 June 2023, San Diego, CA and Online
AIAA AVIATION 2023 Forum

10.2514/6.2023-3646

Darrieus wind turbine noise propagation in urban environments

Kartik Venkatraman* Andrea Bresciani † Julien Maillard ‡ Stéphane Moreau § Julien Christophe¶
Christophe Schram‖

von Karman Institute for Fluid Dynamics, 1640 Rhode-St-Genèse, Belgium
Centre Scientifique et Technique du Bâtiment, 38400 Saint-Martin-d'Hères, France
Université de Sherbrooke, 2500 Boulevard de l'Université, Sherbrooke, QC J1K 2R1

The noise radiated from a Darrieus vertical axis wind turbine (VAWT) is propagated in different idealized urban scenes using a 2.5D ray-based engineering method. Noise measurements and simulated Lattice Boltzmann Method (LBM) results from a Darrieus VAWT are employed as a noise source to perform ray tracing around various idealized benchmark urban scenes, ranging from single isolated buildings to multiple building configurations. Noise maps, 1.5 m above the ground and along different vertical planes around the isolated building cases, illustrate the effect of the sound speed gradient, resulting in higher noise levels downwind and producing complex interference patterns. The more realistic LBM source directivity also illustrates the induced asymmetry in noise propagation that can affect more some regions of the buildings. When the wind turbine source is positioned on a high-rise building, lower noise levels near the ground are observed. In multiple building configurations, wind turbines mounted on rooftops exhibit lower noise levels compared to those mounted directly on masts, emphasizing the screening effect of the roof. The model is also applied to a wind turbine in a realistic urban setting around a central square in Grenoble, France, capturing the complex interference, reflection, and diffraction patterns. Such noise maps could be beneficial for the certification of wind turbines installed in urban environments.

I. Introduction

There is a growing interest in siting wind turbines in the urban environment. Small vertical axis wind turbines (VAWTs) appear to be an ideal candidate as they operate independent of wind direction and are shown to have better performance in highly turbulent wind conditions such as those typically encountered in urban areas [1]. The noise footprint of such turbines could play an important role in their acceptance in densely populated areas. Such turbines have different criteria of annoyance compared to typical large-scale wind turbines. Long-range attenuation of high-frequency noise plays a less important role while diffraction of sound around building corners and other urban noise propagation factors are more important. Several studies have been performed on the importance of the canyon effect in urban noise propagation [2]. Most models for noise propagation in urban environments utilize a ray-based approach and an engineering model as they are quick and accurate for problems involving refraction and diffraction around buildings and complex urban canyons. For instance, Hou *et. al* [3] used a 3D ray tracing model for traffic barriers, road, and railway noise simulations considering different vehicle source emission models. Lee *et. al* [4] investigated the noise amplification due to multiple reflections that occur between high and parallel walls of an urban canyon. Bian *et. al* [5] used a Gaussian beam tracing (GBT) approach to investigate drone and UAM (urban air mobility) noise considering different virtual flight paths. The sound map also depends on the street type and width and decreases in noise levels with logarithmic distance from the source [2]. The level of noise absorption in an urban environment depends on the ground pavement and on the construction material of the building facades which typically comprise brickwork, concrete, and glass. Windows enhance noise absorption at lower frequencies [2]. The directivity of the noise source also plays an important role in the noise radiation patterns around urban canopies. Casalino *et. al* [6] also showcased the potential of LBM/VLES (Lattice Boltzmann Method/Very Large Eddy Simulation) modeling in estimating noise impacts from UAM vehicles for an urban environment. This approach could be computationally intensive, potentially rendering it impractical depending

*PhD candidate, Environmental and Applied Fluid Dynamics dept., 72 chaussée de Waterloo.
†PhD candidate, Centre Scientifique et Technique du Bâtiment, 38400 Saint-Martin-d'Hères, France
‡Senior Research Engineer, Centre Scientifique et Technique du Bâtiment, 38400 Saint-Martin-d'Hères, France
§Professor, Université de Sherbrooke, 2500 Boulevard de l'Université, Sherbrooke, AIAA Senior Member.
¶Senior Research Engineer, Environmental and Applied Fluid Dynamics dept., 72 chaussée de Waterloo, AIAA Senior Member.
‖Professor, Environmental and Applied Fluid Dynamics & Aeronautics and Aerospace depts, 72 chaussée de Waterloo, AIAA Senior Member.

on the frequency range and propagation distance. More recently, Yunus *et. al* [7] presented a new framework focused on GBT within an in-homogeneous atmospheric flow for a urban canopy taking into account the refraction effects due to both vertical and horizontal variations in wind velocity and air temperature. The study demonstrated that in the presence of mean flow, the direct and reflected waves can follow distinct ray paths compared to those in a quiescent atmosphere, leading to unique diffraction patterns in an urban canopy setting. However, none of the existing literature has focused on investigation of the acoustic impact of Darrieus VAWTs sited on a urban rooftop or urban canopy.

For the present study, the noise measurements from field experiments and numerical simulations of various vertical axis wind turbine rotors are fed as an input to a 2.5D ray-based engineering method [8–10] to calculate the noise emissions in urban environment. First, the influence of wind speed on a turbine with available field test data on the QR5 turbine is studied for different urban geometry configurations. Second, the influence on urban noise propagation of the VAWT geometry and the noise directivity pattern obtained from a numerical simulation [11, 12] is investigated.

This methodology could be used to develop noise exposure maps for the certification of urban wind turbines, which are governed by IEC 61400-2013 standard and could be used to test the noise impact of different wind turbine architectures in the early design phase. The present requirements demand a sound emission map and the declared sound power level at a wind speed of 8 m/s [13].

The paper is organized as follows: the different urban scenes used in this work are described in Section II followed by the far-field propagation model in Section III. The input data for the noise source directivity is discussed in Section IV. The results are presented in Section V in terms of sound maps for different geometry conditions using the field measurements. Finally, the conclusions are drawn in Section VI.

II. Building geometry

Different building geometry cases are investigated as defined by the Architectural Institute of Japan (AIJ) [14]. These are benchmark geometries used for the validation of numerical simulations predominantly for the pedestrian wind environment used for comparison of different modelling approaches. First, two single building configurations are investigated: a single high-rise building of dimensions 20 m x 10 m 10 m as shown in Fig. 1 (a) and then a single high-rise building of size 80 m x 10 m x 80 m shown in Fig. 1 (b). Next multiple building configurations are investigated as seen in Fig. 2. Case A seen in Fig. 2 (a) comprising 10 cubic buildings of the same height of 20 m x 20 m x 20 m. Case B shown in Fig. 2 (b) comprising 9 cubic buildings without the central building from Case A. Finally, Case C shown in Fig. 2 (c) comprises 10 cubic buildings, with the central building twice the height (40 m) of the rest of the buildings. The spacing between the buildings is 20 m. The python package Pyvista [15] is utilized for creating the building scene and plotting the sound maps shown in Section V. Finally, the methodology is applied to a real urban environment, corresponding to *Place Victor Hugo*, in the city center of Grenoble, in France. A satellite image and the modelled noise propagation scene is shown in Fig. 3.

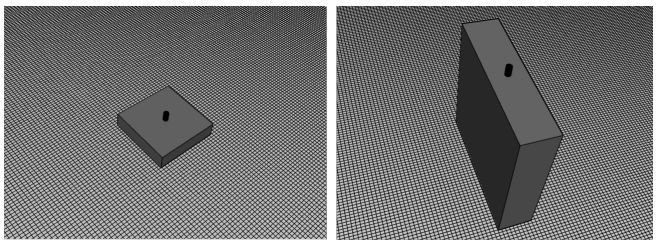

Fig. 1 Isolated building geometry cases a) Case 1 , b) Case 2.

III. Far-field propagation model

The present work uses the 2.5D ray-based engineering method implemented in MithraSIG and MithraSound [8, 9]. The wind turbine is modeled as a point source with prescribed directivity, either mounted on top of a 20 m mast or above the roof of a building. The model involves two steps. First, a 2D ray tracing is executed in the horizontal plane: the ray paths between source and receiver are computed accounting for the reflections due to vertical surfaces (e.g. building facades) and diffraction from vertical and horizontal edges. In the next step, the Harmonoise method [9, 10] is utilized

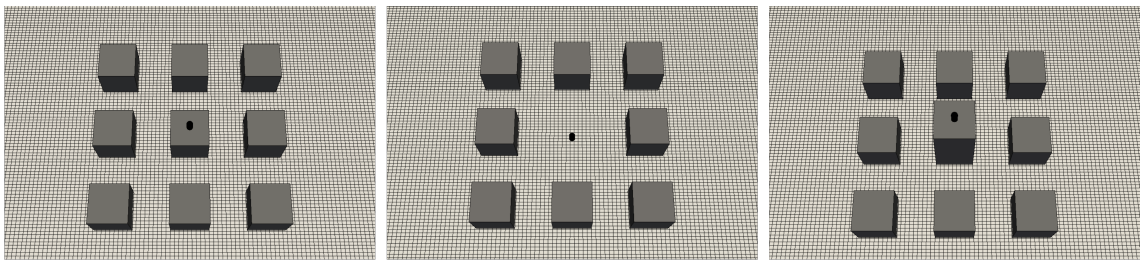

Fig. 2 Building geometry a) Case A , b) Case B and c) Case C.

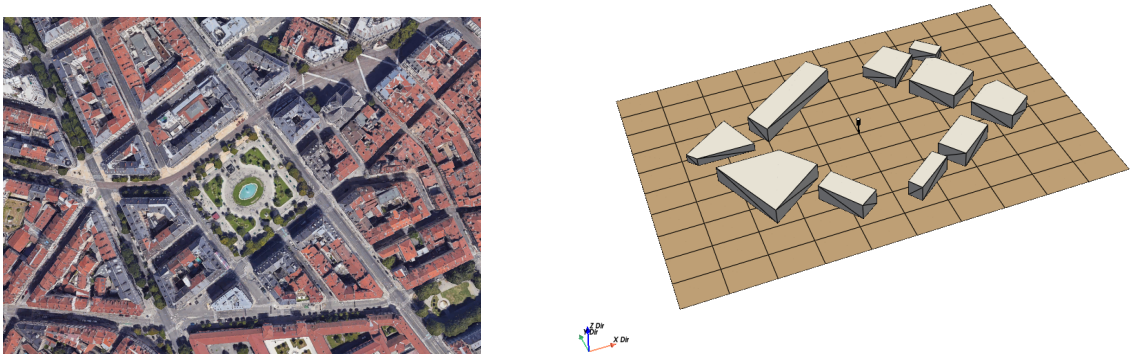

(a) Satellite image **(b) Noise propagation scene**

Fig. 3 Scene showing a) Place Victor Hugo, Grenoble, satellite image taken from Google Earth and b) Noise propagation scene with the buildings around the central square along with a wind turbine sited at the centre.

in the vertical plane comprising the source and the receiver to estimate the noise levels in third-octave bands. The sound pressure level at a $L_{p,xy}$ for each third-octave band due to the source x at the receiver y is

$$L_{p,xy} = L_{w,x} + DI_{xy} - A_{E,xy} \tag{1}$$

where $L_{w,x}$ is the sound power of the source x, and DI_{xy} the directivity gain of the source x in the receiver y direction. The term $A_{E,xy}$ is defined as the excess attenuation:

$$A_{E,xy} = \left[A_{\text{div}} + A_{\text{atm}} + A_{\text{gr+building}} + A_{\text{sc}} + A_r\right]_{xy} \tag{2}$$

It represents a sum of the excess noise attenuation due to spherical divergence, atmospheric absorption, ground and building reflection and diffraction, scattering by atmospheric turbulence, and vertical surface reflections. In the present case, a constant flow resistivity $\sigma = 2000$ kPa s/m^2 is used for the ground (modelled as asphalt). The building facades have been modeled with concrete with constant flow resistivity $\sigma = 20000$ kPa s/m^2. With regards to atmospheric conditions, the Harmonoise meteorological model [16] is used with wind speeds ranging from 7 m/s to 10 m/s and stability class 1, corresponding to a sunny day (unstable atmospheric conditions).

IV. Input noise directivity

Two noise directivity source models could be used as input to the model. The first one is described in Section IV.A and is based on single point measurements for several wind speeds. A uniform directivity is assumed in this case. The second approach is described in Section IV.B and it is based on a numerical simulation.

A. Field test data

The QR5 turbine is a 6.5 kW rated helical Darrieus VAWT, of diameter 3.1 m and height 5.5 m. The noise spectra from the field test measurement of the QR5 turbine are taken from [17–19]. The field test was performed in a relatively

open field. The measurements were taken at a distance of 22.5 m away from the turbine on the ground at wind speeds ranging from 7 m/s to 10 m/s with a relatively constant tip Speed Ratio (ratio of rotational speed to incoming wind speed). Wind speed and direction were recorded every 1 minute to determine the one-third octave band spectra shown in Fig. 4. Further details are provided in [18, 19]. A uniform noise directivity and is used as an input for the noise propagation around different building configurations in Section V.

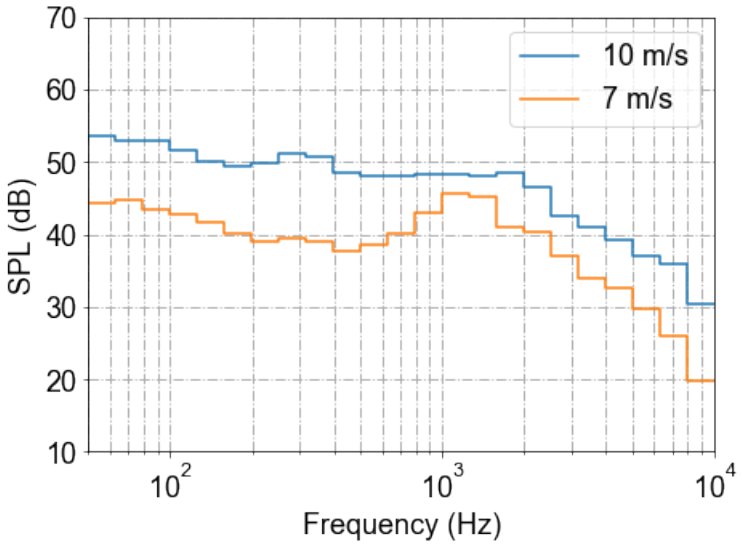

Fig. 4 Field measurement data for the QR5 wind turbine taken at different wind speeds at a distance 22.5 m away [17, 18].

B. Numerical simulation data

Alternatively, a numerical model can be used to compute the noise directivity for a H-Darrieus VAWT configurations as shown in Fig. 5. A 1:5 scaled H-Darrieus wind turbine with end plates and supporting structures is simulated using the LBM-VLES approach [11, 12, 20, 21]. The experimental data from [22] are used to validate the numerical simulation. The parameters of the wind turbine are outlined in Table. 1. The noise directivity from these wind turbines is calculated using the Ffowcs Williams and Hawkings (FW-H) analogy for a sphere of observers located 1 m away from the wind turbine, as shown in Fig. 5. The noise spectra are then scaled to obtain the noise spectra for a full size model using a scaling (similar to [23]) for the sound pressure level based on a dipolar scaling for the wind turbine geometry and rotational speed:

$$SPL_{full} = SPL_{scale} + 60 \times \log((\Omega_{full}/\Omega_{scale}).(D_{scale}/D_{full}).(H_{scale}/H_{full}))$$

The frequency is also scaled based on the Strouhal number to obtain the noise spectra for a full size turbine that could be easily installed on a building rooftop with minimal noise annoyance:

$$f_{full} = f_{scale}.(U_{scale}/U_{full}).(D_{full}/D_{scale})$$

The scaled spectrum in 1/3-octave bands is shown in Fig. 6 and used in Section V for evaluating the impact of a non-uniform directivity on noise propagation for a single square building.

Table 1 Geometrical and operational parameters for a H-Darrieus VAWT turbine

Parameter	Diameter (D)	Height (H)	Rotational speed (Ω)	Inflow speed (U)
Scale model (1:5)	0.2 m	0.2 m	3500 RPM	21.28 m/s
Full size	1 m	1 m	140 RPM	4.2 m/s

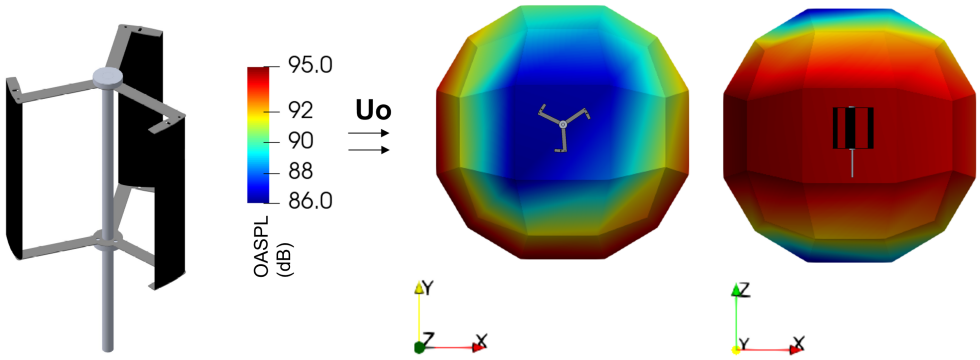

Fig. 5 Noise directivity for a 1:5 scale H-Darrieus wind turbine in the operational regime [11].

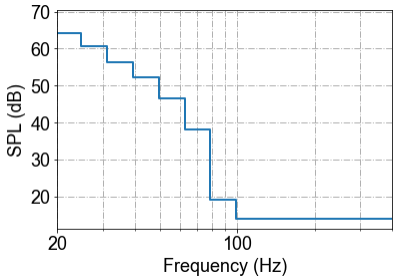

Fig. 6 Noise spectrum for a small H-Darrieus wind turbine in the operational regime scaled to a full scale model [11] shown for a single observer location.

V. Results

The results are shown for urban noise propagation through different building configurations. Firstly, in Section V.A and V.B, a single square building (Case 1) is analyzed to explore the impact of factors such as wind speed, varying thermal stability, and different noise directivity on noise propagation. Next, in Section V.C multiple building configurations are examined to analyze the effects of interference and scattering on noise propagation. The methodology is then applied in Section V.D to a real-world case study of the central square 'Victor Hugo' in Grenoble, France.

A. Single Square building

1. Field Test Data at 10 m/s

The overall scene for the single square building Fig. 7, showing the single square building with a rooftop mounted turbine. The upwind direction is shown along with the horizontal and vertical planes (XY, YZ and XZ) over which the noise maps are plotted. Fig. 8 shows the noise maps in A-weighted Decibel scale (dBA) in the X-Y plane at three different heights, 1.5 m, 10 m and 25 m above the ground using the field-measured noise spectra measured at a wind speed of 10 m/s. The effect of the sound speed gradient on the noise propagation is evident for the plane closer to the ground. In particular, higher noise levels upto 10 dBA are predicted downwind. At the pedestrian level (1.5 m) the noise levels are below 50 dBA. Close to the building, the levels are lower as a result of the screening effect of the roof. The attenuation of noise levels due to the spherical spreading is evident at a height of 10 and 25 m above the ground level. Similarly, noise exposure maps are shown in the vertical planes in Fig. 9. The screening effect of the building can be clearly seen in both planes. Higher noise levels are seen downwind close to the ground in the X-Z plane.

To understand the interference effects that are observed in the vertical planes shown in Fig. 9, the noise spectra are plotted at the different receiver points shown in black in the X-Z plane (shown in Fig. 9a). The noise spectra in third octave bands at different distances from the wind turbine are plotted in Fig. 10. The effect of atmospheric absorption is relevant at high frequencies beyond 2000 Hz showing the decay in noise levels. At lower and mid-frequencies, the scattering, interference, and diffraction effects of the buildings' edges and corner play a key role in the reduction in

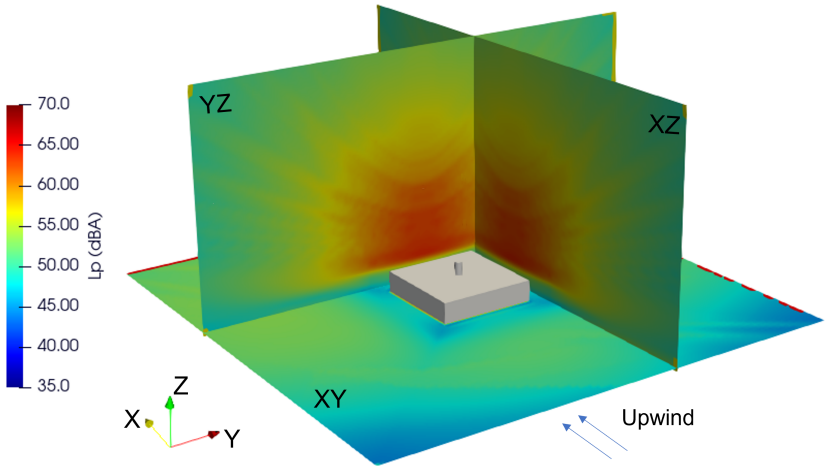

Fig. 7 Setup for single building case showing the orientation of wind flow and definition of different planes.

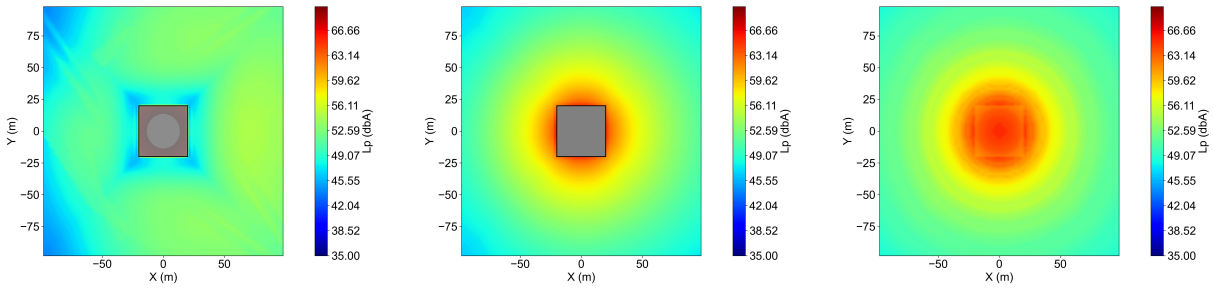

(a) 1.5 m **(b) 10 m** **(c) 25 m**

Fig. 8 Sound map for receivers located in the X-Y plane for single square building (Case 1) at different distances: (a) 1.5 m (pedestrian level), (b) 10 m (building rooftop), and (c) 25 m. (wind blowing from left to right)

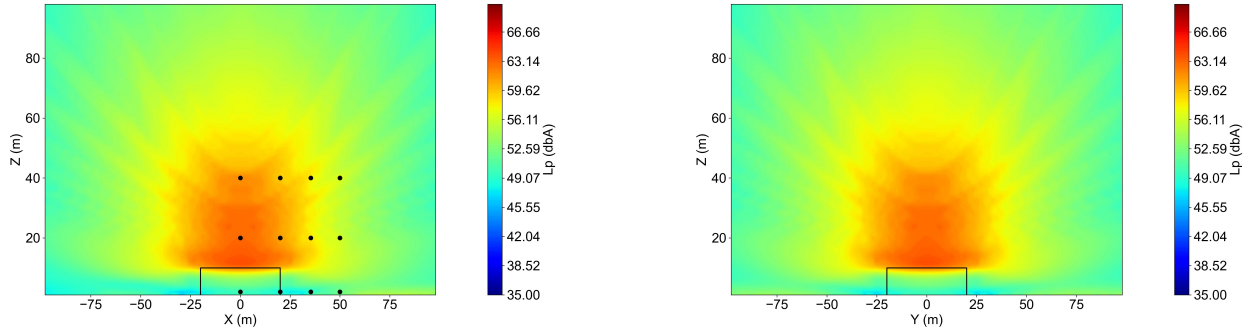

(a) X-Z Plane 25 m **(b) Y-Z Plane 25 m**

Fig. 9 Sound map for receivers located at a distance of 25 m from the center of the turbine in a) X-Z plane and b) Y-Z plane.

noise levels in specific frequency bands dependent on the position. A complete decay in noise levels due to the building acting as a screen is seen at the ground level for all the distances. On the other hand, at heights of 20 m and 40 m, attenuations ranging from 5 to 10 dBA are seen at specific frequency bands at receiver positions further away from the turbine yielding the complex scattering patterns seen in the noise maps.

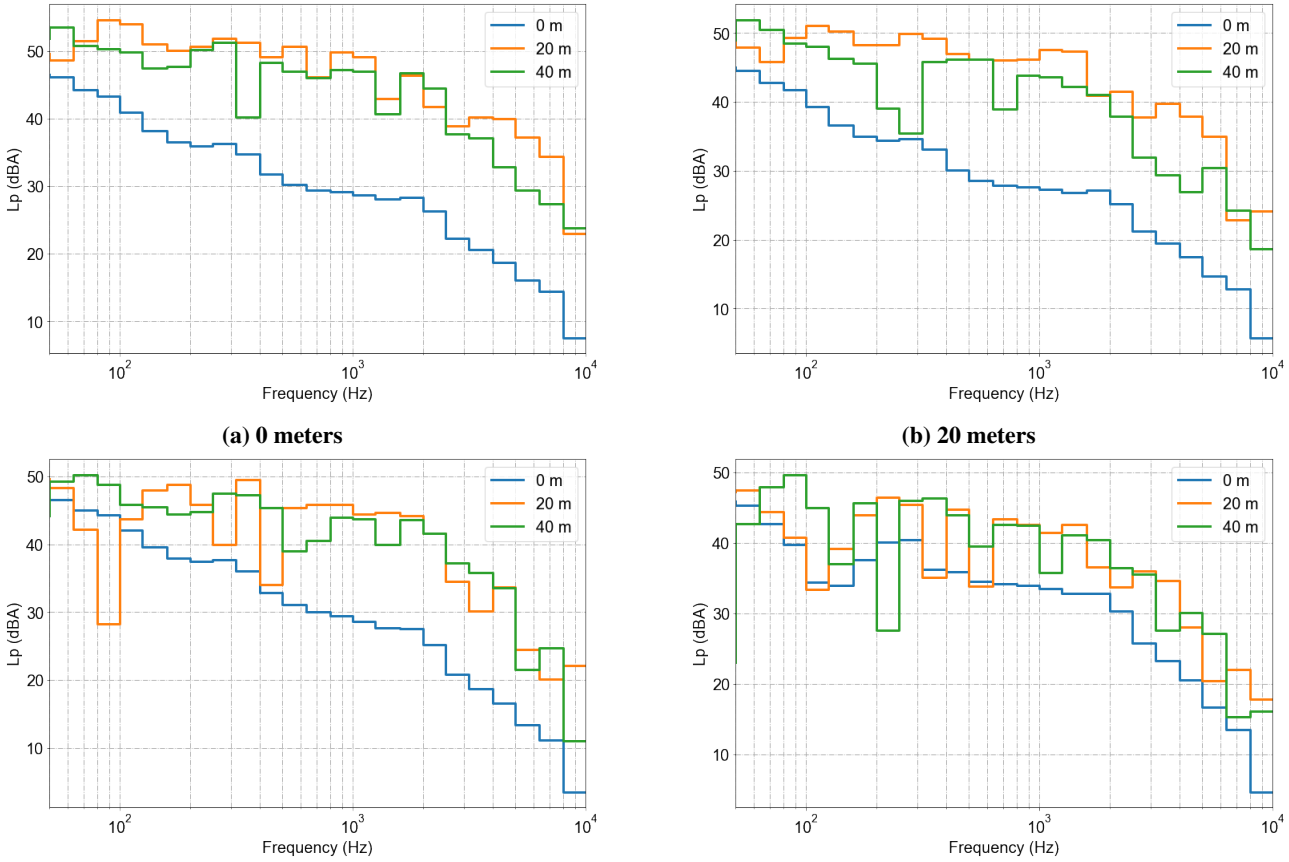

(a) 0 meters **(b) 20 meters**

(c) 35 meters **(d) 50 meters**

Fig. 10 Noise spectra in third octave bands corresponding to points sampled in the X-Z plane shown above at (a) 0 m, (b) 20 m (c) 35 m, and (d) 50 m away from the turbine at different heights (0 m, 20 m and 40 m).

2. Field Test Data at 7 m/s

Similar to the previous case, the noise spectra from field measurement data for a wind speed of 7 m/s is used to evaluate noise exposure maps at a lower wind speed. Fig. 11a shows the noise maps at a pedestrian level of 1.5 m above the ground in the X-Y plane. Low noise levels below 45 dBA is seen over the ground plane spanning 100 m in both directions. A wind turbine operating with this wind speed could satisfy the noise regulations for urban environments that are more stringent at night (below 50 dBA for most European cities [24]). A noise curtailment strategy could be proposed limiting the operational speed of the turbine. Fig. 11b shows the spreading of noise levels in the vertical X-Z plane, showing a different scattering pattern with lower noise levels compared to Fig. 9b shown for a wind speed of 7 m/s. Furthermore, the noise spectra are shown in Fig. 12 at the same sampling points defined earlier at different distances from the wind turbine over several heights. Similar to the spectra for a wind speed of 10 m/s, a reduction of 5 to 10 dBA is seen over different frequency bands due to different interference and diffraction resulting in to the noise map shown over the vertical plane.

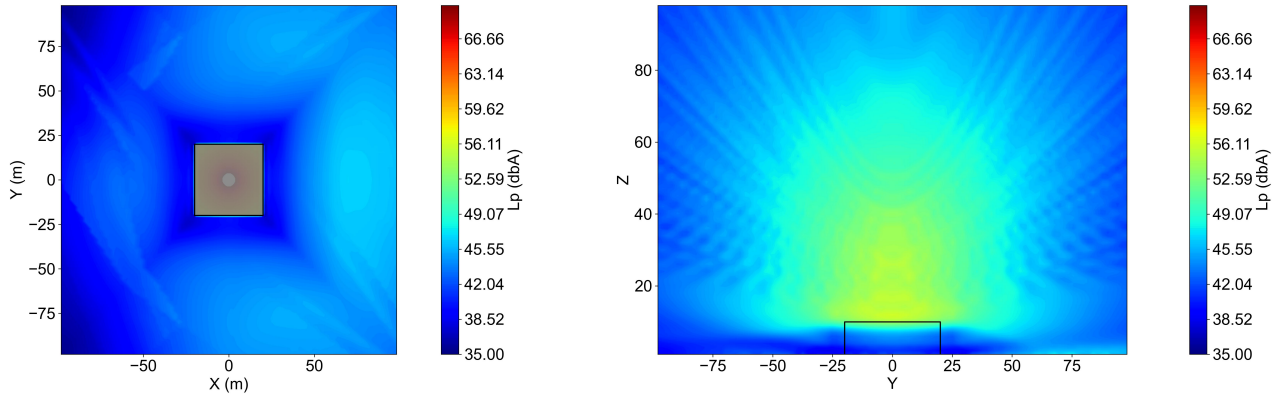

(a) X-Y plane 1.5 m **(b) X-Z plane 25 m**

Fig. 11 Noise Maps for receivers located at different planes for a single square building, using a wind turbine source at a wind speed of 7 m/s.

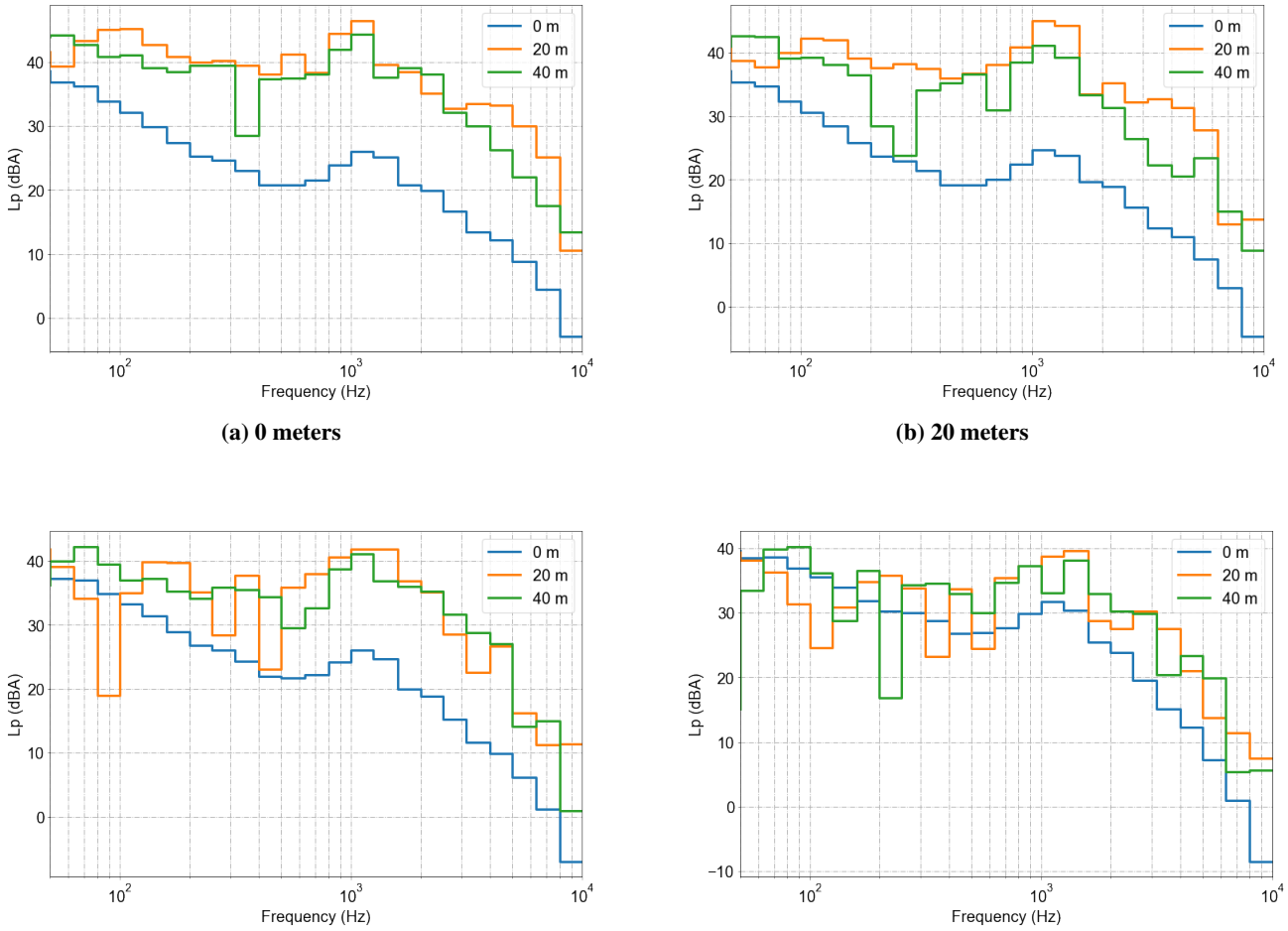

(a) 0 meters **(b) 20 meters**

(c) 35 meters **(d) 50 meters**

Fig. 12 Noise spectra in third octave bands corresponding to points sampled in the X-Z plane shown above at (a) 0 m, (b) 20 m (c) 35 m, and (d) 50 m away from the turbine at different heights (0 m, 20 m and 40 m).

3. Noise directivity from a numerical simulation

The noise directivity shown in Fig. 5 from the numerical simulation results presented in [21] is used to investigate the effect of non-uniform directivity on urban noise propagation for a small H-Darrieus VAWT installed on the rooftop. An asymmetric noise map is seen corresponding to the orientation of noise directivity of the H-Darrieus VAWT as shown for the horizontal plane in Fig. 13a and for the vertical plane shown in Fig. 13b.The increase of the noise levels in the downwind direction caused by the sound speed gradient is partly balanced by the lower noise levels emitted by the wind turbine in the same direction, highlighting the importance of accounting for the non-uniform directivity of the noise source.

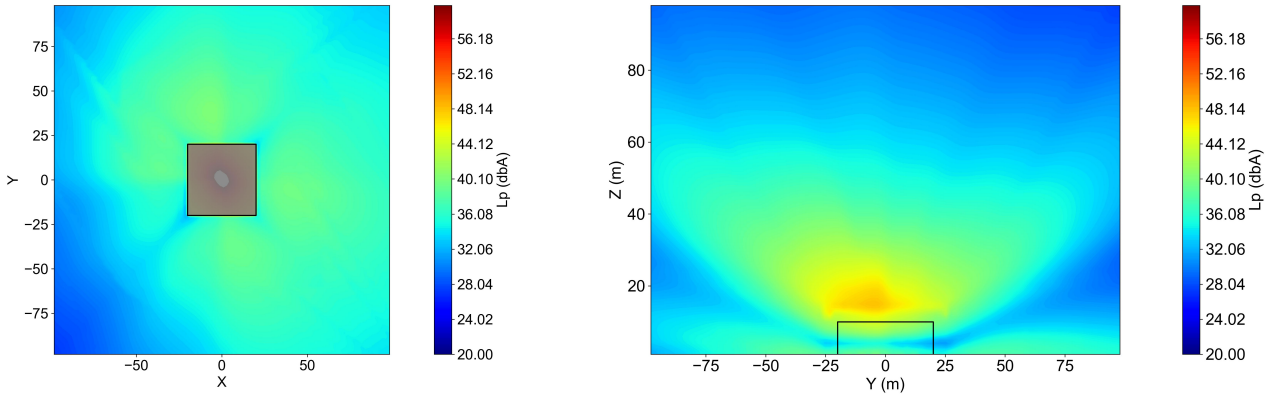

(a) X-Y plane 1.5 m **(b) X-Z plane 25 m**

Fig. 13 Sound maps for noise directivity for a H-Darrieus VAWT from a numerical simulation, shown for a) X-Y plane 1.5 m and b) Y-Z plane 25 m for a wind speed of 4.2 m/s.

For the rest of the study however, a uniform noise directivity source from the field test data at 10 m/s is used to investigate the impact of different building configurations.

B. Single rectangular high rise building

Figs. 14a and 14b show the noise maps in the horizontal plane at heights of 1.5 and 80 m. The wind turbine is installed installed on a single rectangular high rise building. Close to the ground, the noise levels are lower in the direction perpendicular to the wind thanks to the screening effect of the rooftop. A wind turbine deployed on a high-rise could be preferred not only due to its aerodynamic advantages but also due to lower noise annoyance close to the ground. A spherical propagation of noise is seen at 80 m corresponding to the plane near the building rooftop. Additionally, noise maps are plotted in the vertical planes shown for the vertical planes corresponding to the short and long sides of the building in Figs. 15a and 15b, respectively. The noise contours indicate the strong screening effect of the building reducing the noise levels close to the ground. These plots are also useful to understand the noise annoyance close to the building facade and vertical extent of the building over which the noise levels could be unacceptable.

C. Multiple building configurations

The noise maps for the multiple building cases are shown at a pedestrian level (1.5 m) in Figs. 16, 17 and 18 for Cases A, B and C respectively. Similar to the isolated building cases, the wind gradient effect is noticed, with lower noise levels upwind. The vertical edges of the buildings provide additional screening, reducing the noise levels. When the wind turbine is installed at the ground level, i.e. case B shown in Fig. 17, high noise levels are observed in the central square. This is also attributed to the reflection from the building facades. Lower noise levels are noticed for Case C (Fig. 16) compared to Case A (Fig. 18), as expected for a wind turbine placed on a higher building. The noise reaching the building facades is an important indicator to assess the indoor acoustic annoyance. Figs. 20a, 20b and 20c show the noise contours on vertical Y-Z plane for Cases A, B and C, respectively. The simulated scenes along with the plane are shown in Figs. 19a, 19a, 19a respectively. In general, higher noise levels of at least 5 dBA are predicted on the

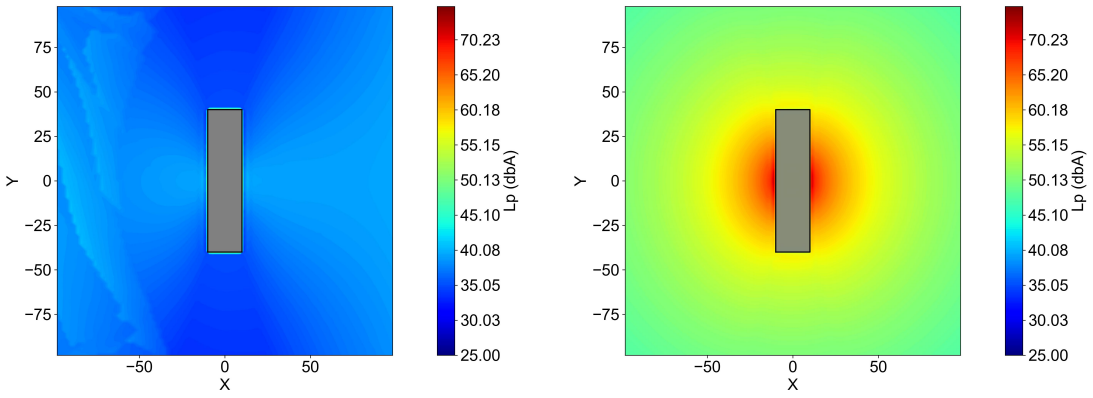

(a) X-Y plane 1.5 m **(b) X-Y Plane 80 m**

Fig. 14 Sound map for receivers located in the X-Y plane a) 1.5 m and b) 80 m above the ground for a wind turbine installed at the centre of a rectangular high rise building.

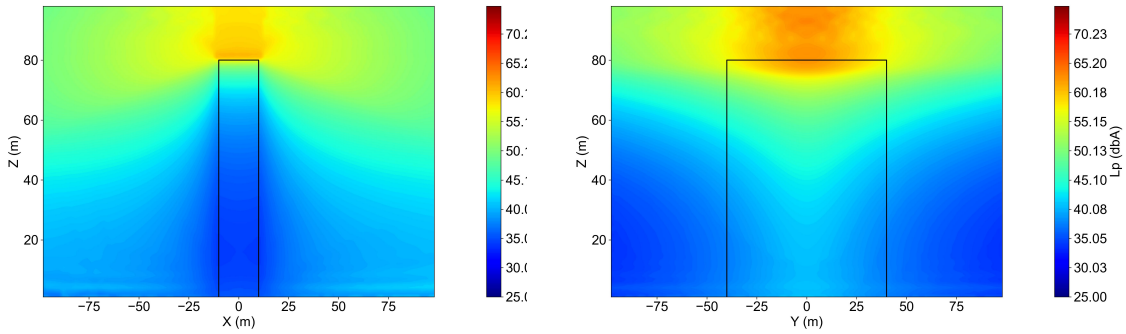

(a) X-Z plane 25 m **(b) Y-Z plane 25 m**

Fig. 15 Sound maps for receivers located in a) X-Z plane at 25 m and b) Y-Z plane at 25 m from a wind turbine installed at the centre of a rectangular high rise building.

facade of the central building that directly faces the wind turbine. In Case B the levels are the highest due to absence of the screening effect of the building. For Case A, the shielding effect of the central building reduces the noise levels below a certain height of the building, while for Case C the shielding effect reduces the noise levels over the entire building height for the surrounding buildings.

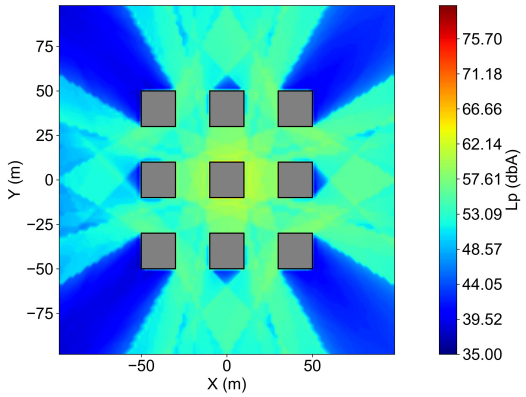

Fig. 16 Sound map for receivers located in a plane 1.5 m above the ground for Case A corresponding to 10 cube buildings of the same height, with a wind turbine installed on the central building.

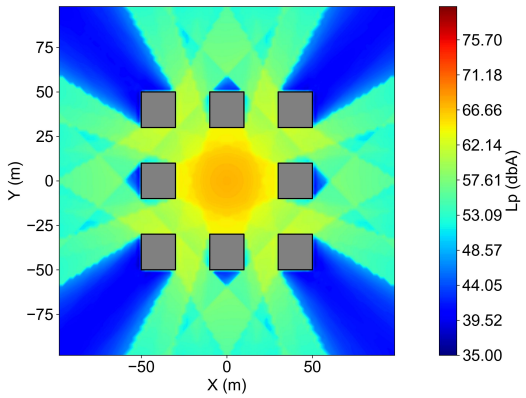

Fig. 17 Sound map for receivers located in a plane 1.5 m above the ground for Case B corresponding to 9 cube buildings with the wind turbine located at the center mounted on a mast.

D. Realistic building configuration

Finally, the noise propagation around a realistic building configuration is investigated for a real urban environment. The urban landscape is shown in Fig. 3 and it represents Victor Hugo Square in Grenoble, France. The VAWT is in the center of the square, 22.5 m above ground (mounted on a 20 m mast). Fig. 21 shows the contours of the noise levels in the horizontal plane 1.5 m above the ground. The sound maps exhibit complex scattering and interference features, the spherical spreading of noise levels around the turbine impacting the building facades directly facing the turbine.

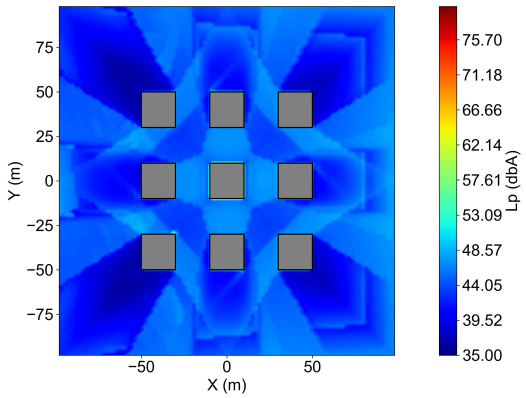

Fig. 18 Sound map for receivers located in a plane 1.5 m above the ground for Case C corresponding to 10 cube buildings with the central building twice the height with roof-mounted wind turbine.

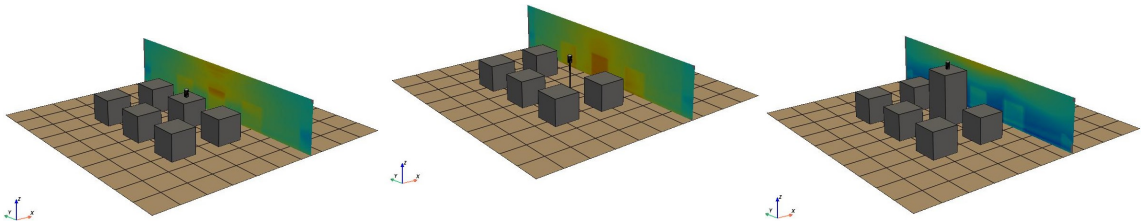

(a) Scene A **(b) Scene B** **(c) Scene C**

Fig. 19 Sound maps showing the setup of three different scenes for Cases A, B, and C.

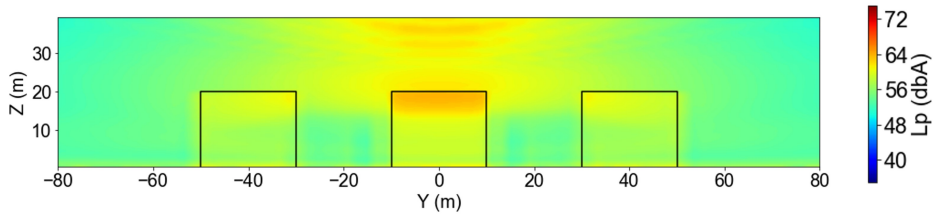

(a) Scene A - Y-Z plane 29 m

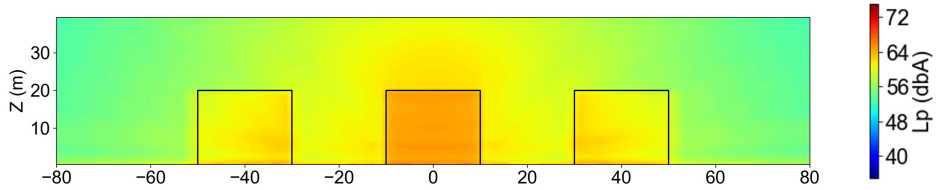

(b) Scene B - Y-Z plane 29 m

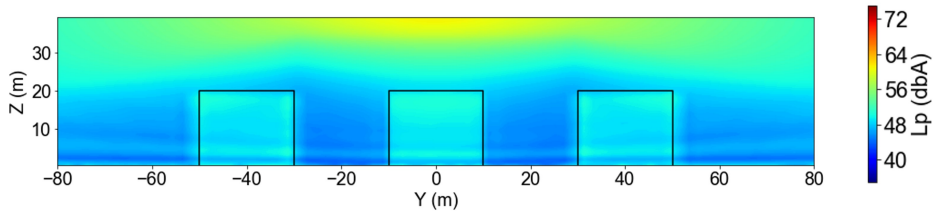

(c) Scene C - Y-Z plane 29 m

Fig. 20 Noise maps in the Y-Z plane close to the building facade for Cases A, B, and C.

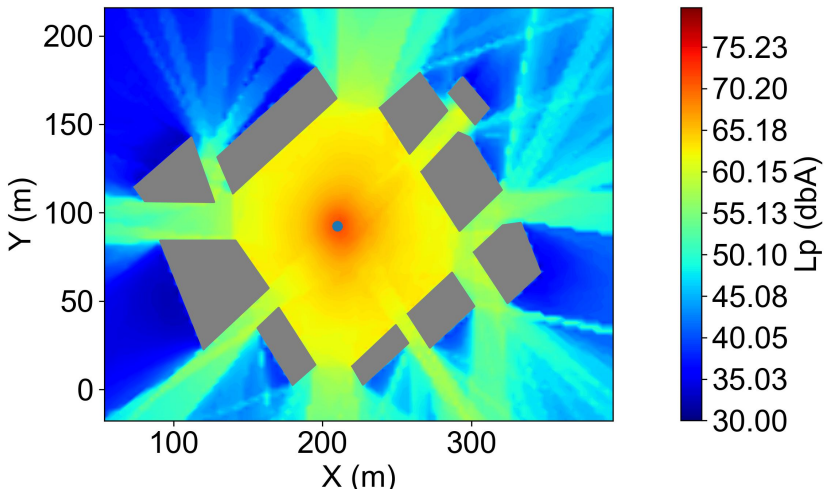

Fig. 21 Sound map for receivers located in the X-Y plane 1.5 m above the ground.

VI. Conclusions

A simulation model chain for urban noise propagation is set up using the ray-tracing engine of MithraSIG and MithraSound and the Harmonoise method. Different benchmark urban cases are simulated from single isolated buildings to multiple building cases and realistic building configurations. The noise maps depict the wind gradient, complex noise reflection, and diffraction effects around buildings. Field measurement data on a helical Darrieus VAWT is used as a uniform noise directivity source for investigating the noise maps at two different wind speeds for a single square building. Higher noise levels are seen downwind compared to upwind, showing the effect of wind gradient. For single isolated building cases, the building acts as a screen reducing the noise footprint at a pedestrian height of 1.5 m above the ground. At higher locations above the ground, the spherical spreading of noise levels is seen. In the vertical planes, complex scattering patterns are seen showing sharp attenuation in specific frequency bands depending on the location attributed to the effect of the presence of the building edge and corner reflections, and diffractions. The noise maps for a wind turbine mounted on a rectangular high-rise building indicate show low noise levels that could be within acceptable limits of 50 dBA, illustrating the advantages of installing a wind turbine at a higher location, not only for performance but also for noise impact. Additionally, the maps could also be useful to evaluate the extent of the building facade impacted by higher noise levels. A non-uniform noise directivity from numerical simulation data for a small H-Darrieus VAWT is used to highlight the asymmetry in noise propagation due to a different noise directivity, illustrating that some regions of the buildings could experience higher noise levels dependent on the directivity of the noise source.

Noise maps for urban street configurations shown for Cases A, B, and C, show the complex interference effects and the noise impact for building facades directly facing the wind turbine source. Mounting a wind turbine on the building rooftop is also seen to provide an attenuation on noise levels in the surrounding building facades. Finally, the applicability of the model chain for a Darrieus VAWT source installed in a realistic urban configuration in a square around Place Victor Hugo, Grenoble is shown. Such noise maps can be developed for the certification of urban wind turbines, which can have implications for urban planning and design efforts to mitigate noise pollution for urban wind turbines.

Acknowledgements

The authors acknowledge the European Commission for its financial support through the project H2020-MSCA-ITN-2019 zEPHYR (Grant Agreement No. 860101).

References

[1] Riegler, H., "HAWT versus VAWT: Small VAWTs find a clear niche," *Refocus*, Vol. 4, 2003, pp. 44–46.

[2] Oldham, D., and Radwan, M., "Sound Propagation in City Streets," *Journal of Building Acoustics*, Vol. 1, 1994. doi: 10.1177/1351010x9400100105.

[3] Hou, Q., Cai, M., and Wang, H., "Dynamic modeling of traffic noise in both indoor and outdoor environments by using a ray tracing method," *Building and Environment*, Vol. 121, 2017. doi:10.1016/j.buildenv.2017.05.031.

[4] Lee, P., and Kang, J., "Effect of Height-To-Width Ratio on the Sound Propagation in Urban Streets," *Acta Acustica united with Acustica*, Vol. 101, 2015. doi:10.3813/AAA.918806.

[5] Bian, H., Tan, Q., Zhong, S., and Zhang, X., "Reprint of: Assessment of UAM and drone noise impact on the environment based on virtual flights," *Aerospace Science and Technology*, Vol. 125, 2022, p. 107547. doi:10.1016/j.ast.2022.107547.

[6] Casalino, D., van der Velden, W. C., Romani, G., and Gonzalez-Martino, I., "Aeroacoustic Analysis of Urban Air Operations Using the LB/VLES Method," *25th AIAA/CEAS Aeroacoustics Conference*, American Institute of Aeronautics and Astronautics, 2019, pp. 1–11. doi:10.2514/6.2019-2662, URL https://doi.org/10.2514/6.2019-2662.

[7] Yunus, F., Casalino, D., Avallone, F., and Ragni, D., "Efficient prediction of airborne noise propagation in a non-turbulent urban environment using Gaussian beam tracing method," *The Journal of the Acoustical Society of America*, Vol. 153, 2023, p. 2362. doi:10.1121/10.0017825.

[8] Maillard, J., and Kacem, A., "Auralization applied to the evaluation of pedestrian and bike paths in urban environments," *Internoise*, 2016, pp. 761–794. URL https://www.researchgate.net/publication/339362676.

[9] Salomons, E., van Maercke, D., Defrance, J., and Roo, F., "The Harmonoise Sound Propagation Model," *Acta Acustica united with Acustica*, Vol. 97, 2011, pp. 62–74. doi:10.3813/AAA.918387ls.

[10] van Maercke, D., and Defrance, J., "Development of an Analytical Model for Outdoor Sound Propagation Within the Harmonoise Project," *Acta Acustica united with Acustica*, Vol. 93, 2007, pp. 201–212.

[11] Venkatraman, K., Moreau, S., Christophe, J., and Schram, C., "H-Darrieus vertical axis wind turbine power prediction using the Lattice Boltzmann approach," *56th 3AF International Conference on Applied Aerodynamics, Toulouse, France*, 2022.

[12] Venkatraman, K., Moreau, S., Christophe, J., and Schram, C., "Numerical Investigation of H-Darrieus wind turbine aerodynamics at different tip speed ratios," *International Journal of Numerical Methods for Heat and Fluid Flow*, 2023. doi:10.1108/HFF-09-2022-0562.

[13] IEC, *IEC61400-2*, International Electrotechnical Commission, 2013.

[14] AIJ, "Architectural Institute of Japan Guidebook for CFD Predictions of Urban Wind Environment," Available at `https://www.aij.or.jp/jpn/publish/cfdguide/index_e.html`, 2020.

[15] Sullivan, C. B., and Kaszynski, A., "PyVista: 3D plotting and mesh analysis through a streamlined interface for the Visualization Toolkit (VTK)," *Journal of Open Source Software*, Vol. 4, No. 37, 2019, p. 1450. doi:10.21105/joss.01450, URL `https://doi.org/10.21105/joss.01450`.

[16] Defrance, J., Salomons, E., Stuijt, I., Heimann, D., Plovsing, B., Watts, G., Jonasson, H., Zhang, X., Premat, E., Schmich-Yamane, I., Aballéa, F.-E., Baulac, M., and Roo, F., "Outdoor Sound Propagation Reference Model Developed in the European Harmonoise Project," *Acta Acustica united with Acustica*, Vol. 93, 2007, pp. 213–227.

[17] Pearson, C., and Graham, W., "Experimental characterization of vertical-axis wind turbine noise," *The Journal of the Acoustical Society of America*, Vol. 137, 2015, p. EL111. doi:10.1121/1.4904915.

[18] Dyne, B., and S.J.C, "Wind Turbine Noise Measurements," Tech. rep., ISVR Consulting, Institute of Sound and Vibration Research, University of Southampton, 2007.

[19] Botha, J., Shahroki, A., and Rice, H., "An implementation of an aeroacoustic prediction model for broadband noise from a vertical axis wind turbine using a CFD informed methodology," *Journal of Sound and Vibration*, Vol. 410, 2017, pp. 389–415. doi:10.1016/j.jsv.2017.08.038.

[20] Venkatraman, K., Moreau, S., Christophe, J., and Schram, C., "Numerical investigation of the effect of inflow non-uniformity on the noise radiated by a vertical axis wind turbine," *AIAA AVIATION Virtual Forum*, 2021, pp. 1–14. doi:10.2514/6.2021-2216.

[21] Venkatraman, K., Moreau, S., Christophe, J., and Schram, C., "Numerical investigation of the noise radiated by an H-Darrieus vertical axis wind turbine at different tip speed ratios," *28$^{\text{th}}$ AIAA/CEAS Aeroacoustics Conference, Southampton*, 2022, pp. 1–14.

[22] Weber, J., Becker, S., Scheit, C., Grabinger, J., and Kaltenbacher, M., "Aeroacoustics of Darrieus Wind Turbine," *International Journal of Aeroacoustics*, Vol. 14, 2015, pp. 883–902. doi:10.1260/1475-472X.14.5-6.883.

[23] Avallone, F., van der Velden, W. C. P., Ragni, D., and Casalino, D., "Noise reduction mechanisms of sawtooth and combed-sawtooth trailing-edge serrations," *Journal of Fluid Mechanics*, Vol. 848, 2018, pp. 560–591. doi:10.1017/jfm.2018.377, URL `https://doi.org/10.1017/jfm.2018.377`.

[24] Fabris, C., "Noise policy in Germany," *The Journal of the Acoustical Society of America*, Vol. 131, 2012, p. 3295. doi:10.1121/1.4708322.